*Korean J. Chem. Eng.*, 33(10), 2943-2952 (2016)
DOI: 10.1007/s11814-016-0138-y

pISSN: 0256-1115
eISSN: 1975-7220

# A comparative study of $CO_2$ and $CH_4$ adsorption using activated carbon prepared from pine cone by phosphoric acid activation

**Soodabeh Khalili*, Behnam Khoshandam*,†, and Mohsen Jahanshahi****

*Faculty of Chemical, Petroleum and Gas Engineering, Semnan University, Semnan, Iran
**Nanotechnology Institute, Chemical Engineering Department, Babol University of Technology, Babol, Iran
(*Received 17 January 2016 • accepted 14 May 2016*)

**Abstract**−Adsorption of pure carbon dioxide and methane was examined on activated carbon prepared from pine cone by chemical activation with $H_3PO_4$ to determine the potential for the separation of $CO_2$ from $CH_4$. The prepared adsorbent was characterized by $N_2$ adsorption-desorption, elemental analysis, FTIR, SEM and TEM. The equilibrium adsorption of $CO_2$ and $CH_4$ on AC was determined at 298, 308 and 318 K and pressure range of 1-16 bar. The experimental data of both gases were analyzed using Langmuir and Freundlich models. For $CO_2$, the Langmuir isotherm presented a perfect fit, whereas the isotherm of $CH_4$ was well described by Freundlich model. The selectivity of $CO_2$ over $CH_4$ by AC ($CO_2$ : $CH_4$=50 : 50, 298 K, 5 bar), predicted by ideal adsorbed solution theory (IAST) model, was achieved at 1.68. These data demonstrated that pine cone-based AC prepared in this study can be successfully used in separation of $CO_2$ from $CH_4$.

Keywords: Activated Carbon, Pine Cone, Carbon Dioxide, Methane, IAST

## INTRODUCTION

Raw natural gas drilled from gas reservoirs is composed of up to 90% of methane ($CH_4$) and other hydrocarbons depending on the source of the gas in addition to acid gases impurities such as carbon dioxide ($CO_2$) and hydrogen sulfide ($H_2S$). There is a rising global demand for energy, and natural gas (NG) has become a significant energy source [1,2]. Therefore, in order to prevent crystallization during cryogenic processes (liquefaction process) and to increase pipeline gas quality and gas sales specifications, $CO_2$ must also be removed. Consequently, $CO_2$ removal from natural gas will improve the heating value of the gas [3,4].

Separation of carbon dioxide from methane in natural gas can happen through some technologies such as amine absorption, membrane and adsorption. Among these different separation technologies, adsorption method has emerged as a practical and valuable option over conventional techniques like amine scrubbing. The amine solvents have some limitations including volatilization, corrosion and high-energy consumption during the regeneration process, which are the main drawbacks for their long-term application [5-7].

Among all the available porous adsorbents, undoubtedly activated carbon is the most employed material for PSA applications because of its low-cost, high availability, large surface area, microporous structure, easy-to-design pore structure and chemical resistance to acidic and basic conditions [8,9]. The precursor activators and the techniques in production of ACs are useful in the adsorption capacity and their cost. Using natural coal as non-renewable and expensive starting materials and conventional long duration heating production methods caused that commercial activated carbons to be still considered as relatively expensive substances [10,11]. Therefore, finding low-cost and locally available resources as potential alternative precursors is essential in production of activated carbons.

In recent years, many studies have been done in production of AC from biological materials as precursors because of their high adsorption capacity and low cost [12-16]. But there are only few studies about raw pine cone as low cost agricultural by-product in preparation of activated carbon [17,18]. In principle, physical and chemical activation are the two main ways for production of activated carbons. In physical activation, the raw material is placed under a heat treatment at high temperatures in the presence of oxidizing agents, such as carbon dioxide, water steam, or a mixture of them. In the chemical activation process, the raw material and inorganic activating agents such as $H_3PO_4$, $ZnCl_2$, KOH, NaOH, $H_2SO_4$, and $K_2CO_3$ are thoroughly mixed and activated in higher followed by thermal activation in order to create the pore structure [19-21].

To the best of our knowledge, no study has been done on application of pine cone-based activated carbon in order to investigate the separation of $CO_2$ from $CH_4$. Hence, in this study, pine cone was used as a precursor to prepare activated carbon by chemical activation method using phosphoric acid as an effective activation agent for preparation of highly porous carbon. The adsorption equilibrium data of pure $CO_2$ and pure $CH_4$ on prepared activated carbon were measured volumetrically at different temperatures (298, 308 and 318 K) and pressures ranging 1 to 16 bar. The equilibrium, kinetic and thermodynamic study of the $CO_2$ and $CH_4$ adsorption were studied to describe the adsorption processes.

†To whom correspondence should be addressed.
E-mail: bkhoshandam@semnan.ac.ir

## MATERIALS AND METHODS

### 1. Materials

The precursor, pine cone, used for the preparation of activated carbon was obtained from Semnan province, Iran. Carbon dioxide, methane, helium and nitrogen with purity of 99.99%, 99.995%, 99.995% and 99.995%, respectively, were purchased from Technical Gas Services, UAE. Phosphoric acid 85% ($H_3PO_4$) and Hydrochloric acid 37% (HCl) were obtained from Scharlau.

### 2. Characterization of the AC Precursor

The moisture, ash content and volatile matter of the precursor (pine cone) were defined using a standard method according to ASTM D2867, ASTM D2866-94 and ASTM D5832-98, respectively. An elemental analysis of carbon, hydrogen, nitrogen, sulfur was done by using a Costech ECS 4010 elemental analyzer. The percentage of oxygen was calculated by the difference between 100% and sum of carbon, hydrogen, nitrogen, sulfur and ash.

### 3. Preparation of Activated Carbon

Pine cones were washed with distilled water several times to eliminate dust and impurities and then placed in an oven overnight at 110 °C. The cleaned pine cones were ground and sieved by the mesh number 60. The dried pine cones were impregnated with a weighed amount of $H_3PO_4$ aqueous solution and stirred continuously at 80 °C for 3 h. After mixing, the slurry was dried in vacuum drying at 110 °C for 20 h. The resultant mixture was introduced in tubular quartz and subjected to heat up to the desired temperature about 500 °C with a rate of 5 °C/min and holding time of 170 min in an electrical furnace under a nitrogen flow rate of 100 mL/min STP.

After cooling to room temperature in a nitrogen flow, the prepared adsorbent was removed from the reactor. The product of pyrolysis was washed sequentially with solution of HCl (0.5 M), hot water and finally cold distilled water until the pH value of the filtrate was around 6.0 and then dried at 110 °C overnight.

### 4. Characterization of the Prepared Adsorbent

Various techniques have been utilized to characterize the synthesized AC using different characterization techniques to obtain useful information about its structure. The morphology of prepared AC from pine cone was analyzed by scanning electron microscope (SEM) and transmission electron microscope (TEM) to obtain supplementary information regarding the adsorbent.

The surface functional groups of the sorbent were evaluated by Fourier transform infrared radiation (FTIR) spectrometer (Bruker Vertex-70 FTIR). The spectra were recorded in the range of 400-4,000 $cm^{-1}$ and the potassium bromide (KBr) pellet (Fluka, Co) was applied as reference sample. The moisture, volatile matter and ash content of the prepared activated carbon were determined by using a standard test method according to ASTM D2867, ASTM D5832-98 and ASTM D2866-94, respectively. In addition, the iodine number, which demonstrated the milligrams of adsorbed iodine per gram of AC, was determined by ASTM standard D 4607-94. The content of C, H, N and S in a sample was determined using a Costech ECS 4010 (Italy) elemental analyzer, and the O content was calculated by subtracting the sum of C, H, N and S (%) from 100. $N_2$ adsorption experiments applying BELSORP measuring instruments (BEL, Japan, Inc.) were performed to investigate the textural characterization of the prepared adsorbent from pine cone. The sample was outgassed at 393 K under nitrogen flow for about 15 h prior to BET analysis. The $N_2$ adsorption-desorption isotherms were recorded at 77 K at the relative pressure ($P/P_0$) range of 0.0001-0.99. The specific surface area was determined by using the Brunauer-Emmett-Teller (BET) equation. The micropore size distribution and the mesopore size distribution were determined by micropore analysis method (MP method) and Barrett-Joyner-Halenda (BJH) method, respectively. Also, pore volume was estimated by the liquid volume of adsorption ($N_2$) at a relative pressure of 0.99.

### 5. Experimental Set-up

Adsorption equilibrium of pure gases on synthesized activated

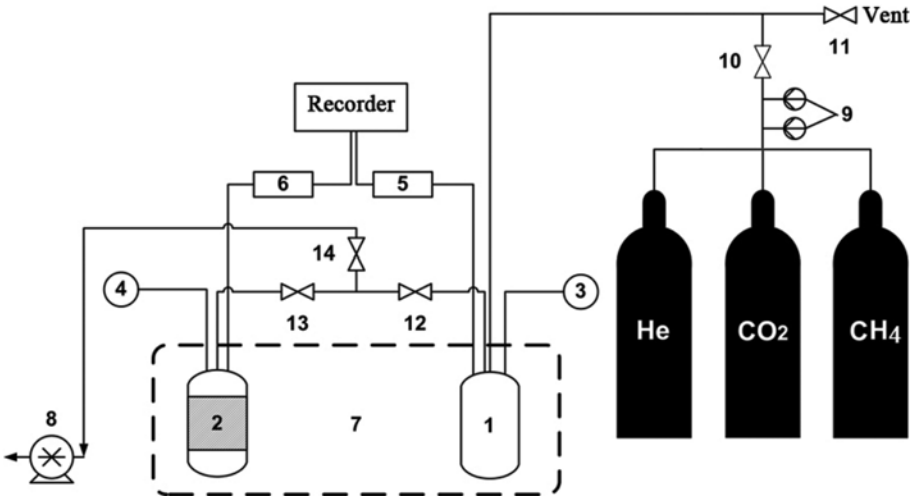


**Fig. 1. Schematic diagram of the volumetric adsorption set-up.**

1. Reference cell
2. Adsorption cell
3, 4. Temperature digital indicator connected to the temperature probe
5, 6. Pressure digital indicator connected to the pressure transducer
7. Water bath
8. Vacuum pump
9. Regulator
10-14. Valves

carbon was performed with a volumetric adsorption apparatus by the setup shown in Fig. 1. The apparatus used for gas adsorption experiments consisted of two high-pressure stainless steel, called sample cell and reference cell.

Before each test, the prepared AC was degassed to eliminate water and other adsorbed gases at 423 K for 24 hours. To keep the temperature of the both cells constant during the adsorption of carbon dioxide and methane, a water bath along with a water circulating system was employed. Prior to measurement, the entire system was vacuumed by vacuum pump for 2 hours. For determination of the dead volume, He gas was applied as non-adsorbing gas. The equilibrium adsorption experiments were performed under different temperatures (298, 308 and 318 K) and pressure range of 1-16 bar. The adsorption capacity was determined by a mass balance at the equilibrium temperature and pressure.

**6. Adsorption Isotherm**

The theoretical Langmuir sorption isotherm assumes monolayer coverage of adsorbate on a homogeneous adsorbent surface. The non-linear equation of Langmuir isotherm model is presented as follows [22,23]:

$$q = q_m \frac{bP}{1+bP} \tag{1}$$

where q is the amount of gas adsorbed per unit mass of AC (mmol·$g^{-1}$); $q_m$ is the maximum adsorption capacity of adsorbent for the gas molecules (mmol·$g^{-1}$) and b is the energy constant.

The Freundlich isotherm model is used for interaction between adsorbed molecules on heterogeneous surfaces and is commonly expressed as follows [24]:

$$q = KP^{1/n} \tag{2}$$

where n is the heterogeneity factor and K is Freundlich constant. For n=1, n<1 and n>1 the adsorption processes are linear, a chemical process and physical process, respectively. In recent cases, the sorption is favorably adsorbed on the adsorbent [25,26].

**7. Kinetic Study**

Two of the most commonly used kinetic models are pseudo-first-order and pseudo-second-order kinetic models [27,28]. The nonlinear form of these two kinetic models can be expressed as follows:

$$q_t = q_e(1-e^{-k_1 t}) \tag{3}$$

$$q_t = \frac{k_2 q_e^2}{1+k_2 q_e t} t \tag{4}$$

where $k_1$ and $k_2$ are the rate constants of Lagergren-first-order and pseudo-second-order adsorption, respectively. The $q_e$ (mmol·$g^{-1}$) denotes the amount of adsorption at equilibrium and $q_t$ (mmol·$g^{-1}$) is the amount of gas adsorbed at time t (min).

**8. Selectivity from the Ideal Adsorption Solution Theory (IAST)**

The other important parameter for evaluation of prepared AC in $CO_2$ separation applications is selectivity for $CO_2$ over other component of the gas mixture. The selective adsorption of $CO_2$ over $CH_4$ can be attributed to two main mechanisms: size exclusion (kinetic separation) and thermodynamic separation. In selectivity based on the size exclusion, the separation occurs based on the size of gas molecule, whereas the thermodynamic separation depends on the difference between physical properties of the gas molecules such as polarizability, or the quadrupole moment [29,30].

The ideal adsorption solution theory (IAST), proposed by Mayer and Prausnitz [31], is a well-known theory for predicting the gas selectivity using only data from the pure component isotherm at the same temperature and on the same adsorbent. The main condition for the IAST application is excellent curve fitting model for single component adsorption data. The main assumption for this theory is that the spreading pressures ($\pi$) are considered equal for all components at equilibrium. Therefore, for a two-component mixture, the spreading pressure is determined as follows [32]:

$$\int_0^{P^0_{CO_2}} \frac{q_{CO_2}}{P} dp = \int_0^{P^0_{CH_4}} \frac{q_{CH_4}}{P} dp = \frac{\pi A}{RT} \tag{5}$$

where A is the surface area of the adsorbent. Raoult's law for both gases is written:

$$Py_{CO_2} = P^0_{CO_2} x_{CO_2} \tag{6}$$

$$Py_{CH_4} = P^0_{CH_4} x_{CH_4} \tag{7}$$

The total number of adsorbed moles is defined by:

$$\frac{1}{qt} = \frac{x_{CO_2}}{q_{CO_2}(P^0_{CO_2})} + \frac{x_{CH_4}}{q_{CH_4}(P^0_{CH_4})} \tag{8}$$

At given $y_i$ and P, the above equations must be solved simultaneously to obtain $x_i$ and $P^0_i$. The adsorption selectivity for carbon dioxide from methane can be determined by the values of $P^0_{CO_2}$, $P^0_{CH_4}$, and $x_{CO_2}/_{CH_4}$ as follows:

$$S_{CO_2/CH_4} = \frac{x_{CO_2}/y_{CO_2}}{x_{CH_4}/y_{CH_4}} \tag{9}$$

where $x_{CO_2}$ and $x_{CH_4}$ are the mole fractions in adsorbed phase and $y_{CO_2}$ and $y_{CH_4}$ are the mole fractions of $CO_2$ and $CH_4$ in gas phase. The larger the selectivity, the easier the separation of $CO_2$ from $CH_4$ by adsorption [33].

**9. Thermodynamic of Adsorption**

The isosteric heat of adsorption of a gas is determined from temperature dependence of the isotherm using the Clausius-Clapeyron equation as follows [34]:

$$\Delta H_{st} = R\left[\frac{d\ln P}{d\left(\frac{1}{T}\right)}\right]_q \tag{10}$$

where $\Delta H_{st}$ (kJ·$mol^{-1}$), T (K), P (bar) and R (J·$mol^{-1}$·$K^{-1}$) are isosteric heat of absorption, absolute temperature, pressure at a constant gas loading of q and ideal gas constant, respectively.

To estimate the influence of temperature on gas adsorption, standard free energy ($\Delta G^0$), entropy ($\Delta S^0$) and enthalpy (isosteric heat of adsorption under isothermal conditions, $\Delta H^0$) were evaluated by the experimental equilibrium data using the following equations [35]:

$$\Delta G^0 = RT\ln\frac{P}{P_s} \tag{11}$$

**Table 1. Ultimate and proximate analysis of pine cone and activated carbon prepared from pine cone**

| Sample | Ultimate analysis (wt%) | | | | | Proximate analysis (wt%) | | | | Iodine number (mg/g) |
|---|---|---|---|---|---|---|---|---|---|---|
| | Carbon | Hydrogen | Nitrogen | Sulfur | *Oxygen | Moisture | Volatile matter | Ash | **Fixed carbon | |
| Pine cone | 47.71 | 6.16 | 0.12 | 1.21 | 42.59 | 9.63 | 79.05 | 2.21 | 9.11 | - |
| AC | 71.32 | 4.30 | 0.00 | 0.90 | 19.73 | 6.50 | 22.04 | 3.75 | 67.71 | 1345 |

*Calculated by difference between 100% and sum of carbon, hydrogen, nitrogen, sulfur and ash
**Calculated by difference between 100% and sum of moisture, volatile matter and ash

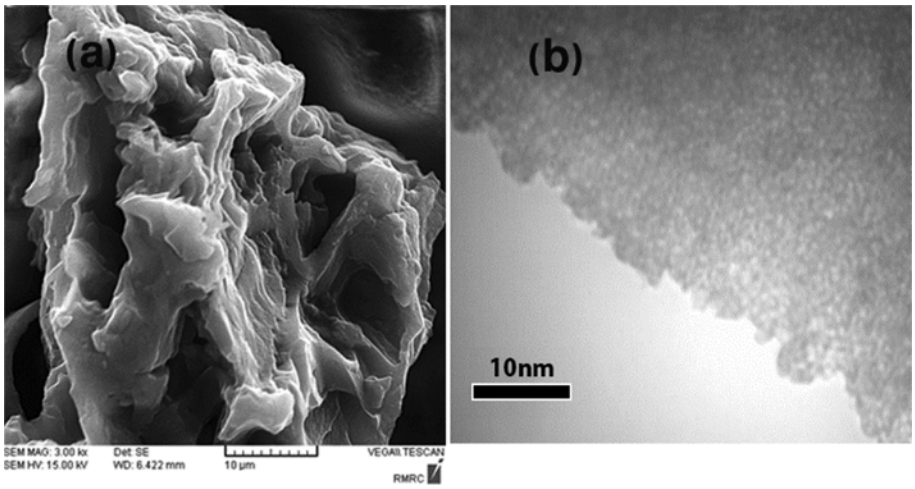


**Fig. 2. SEM (a) and TEM (b) images of prepared activated carbon.**

$$\Delta G^0 = \Delta H^0 - T\Delta S^0 \quad (12)$$

where $P_S$ denotes the equilibrium pressure of the gas at standard pressure (1bar).

## RESULTS AND DISCUSSION

### 1. Material Characterization

1-1. Ultimate and Proximate Analysis

The results obtained from proximate and ultimate analyses of the pine cone and prepared activated carbon are shown in Table 1. The high carbon content, high content of volatile matter and low ash indicated that this precursor is appropriate for preparing activated carbon. After production of activated carbon the carbon and oxygen content was increased and decreased, respectively, because of the partial decomposition of volatile compounds during carbonization process.

1-2. Surface Morphology Analysis

The SEM image of the pine cone-based AC, shown in Fig. 2(a), reveals the porous surface with different size and shapes, confirming relatively high surface area. It appears that the evaporation of the phosphoric acid during carbonization process caused cavities to form on the surfaces of adsorbent. The TEM image of the pine cone-based activated carbon is depicted in Fig. 2(b). From TEM image, the activated carbon has a well-developed porous structure containing inter-connected nanochannels (white fringes), which were created by the disordered packing of turbostratic carbon sheets (black fringes).

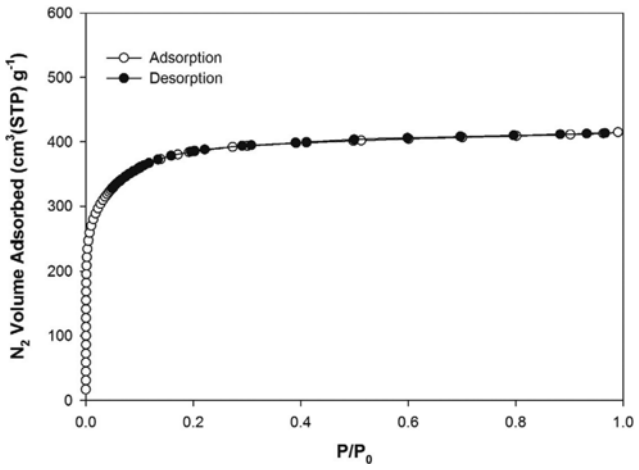


**Fig. 3. Adsorption/desorption isotherms of $N_2$ for prepared AC.**

1-3. BET Analysis

Fig. 3 depicts the $N_2$ adsorption-desorption isotherms of the pine cone-based AC. The sorption isotherm is type I according to the Brunauer classification, which indicates the presence of micropores in the prepared AC and having a relatively small external surface area. Therefore, most adsorption of $N_2$ occurred in low relative pressure region due to the formation of highly micropores in the structure of the AC.

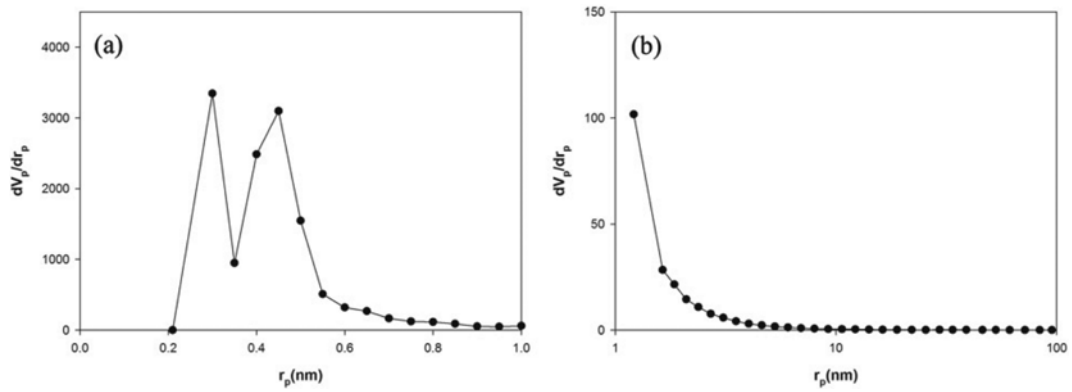


**Fig. 4. Micropore (a) and mesopore (b) size distributions of pine cone-based AC obtained by MP and BJH.**

**Table 2. Textural properties of prepared sample**

| | |
|---|---|
| BET surface area ($m^2$/g) | 1470 |
| Total pore volume ($cm^3$/g) | 0.6415 |
| Micropore volume ($cm^3$/g) | 0.6304 |
| Mesopore volume ($cm^3$/g) | 0.0111 |
| Micropore volume (%) | 98 |
| Average pore diameter (nm) | 1.7452 |
| Micropore width (nm) | 0.7572 |

The pore diameter distribution of micropore obtained from a micropore plot (MP) and mesopore size distribution derived from a Barrett Joyner Halenda (BJH) plot of AC are shown in Fig. 4. The volume distribution ($dV_p/dr_p$) of prepared AC abruptly increased, especially near the micropore region, indicating the presence of numerous micropores with sizes in the ranges of 0.2-1.2 nm. Also, there are some mesopores in the structure of pine cone-based AC. Table 2 demonstrates the structural properties of the AC.

1-4. FTIR Analysis

Fig. 5 illustrates the FTIR spectra of AC. The peak at 1,558 $cm^{-1}$ can be associated with C=C bond in aromatic rings of carbon structure of activated carbon. The peaks at 1,032 and 1,699 $cm^{-1}$ are assigned to C-O-C stretching in ethers and C=O stretching in lactones, respectively. The peaks at 2,853 and 2,923 $cm^{-1}$ are due to the asymmetric and symmetric stretch of -CH group in carboxylic acids. The broad peak at 3,430 $cm^{-1}$ represents the O-H group of phenol, carboxylic acid and alcohol [36,37].

**2. Adsorption Isotherm Simulation**

Fig. 6 demonstrates the equilibrium adsorption isotherms of $CO_2$ and $CH_4$ on the prepared activated carbon from pine cone. Based on the Brunauer classification, all of the $CO_2$ and $CH_4$ adsorption isotherms are Type I. This phenomenon is predictable for adsorption of small adsorbates such as $CO_2$ and $CH_4$ molecules on a microporous adsorbent. Also, it exhibits a steep increase at low pressure due to the existence of vacancies or sites available for adsorption. At higher pressure, the gas adsorbed amounts increase slightly because at high pressure most of the sites are occupied.

Results demonstrated that the adsorption capacity of both gases decreased with increasing the temperature from 298 K to 318 K, indicating the exothermic nature of the $CO_2$ and $CH_4$ adsorption. In fact, as temperature increased, the physical bonding between the gas molecules (including $CO_2$ and or $CH_4$) and the active sites of the adsorbent weakened. Therefore, gas molecules adsorbed on the AC surface obtain enough energy to overcome the van der Waals forces and go back to the gas phase. Consequently, the sorption values decreased with temperature increment.

As can be seen from the equilibrium isotherms, carbon dioxide was the most adsorbed gas and this prepared adsorbent is almost selective to carbon dioxide. This is due to the structure of prepared activated carbon, which is a highly porous material and possesses a distribution of small selective pores that are as the same as the dimension of $CO_2$ molecules. Actually, the separation of $CO_2$ and $CH_4$ molecules by using activated carbon as adsorbent can occur by molecular sieve effect or by selective adsorption. In a binary gas mixture, separation is by selective adsorption and surface diffusion of more strongly adsorbed component, whereas by

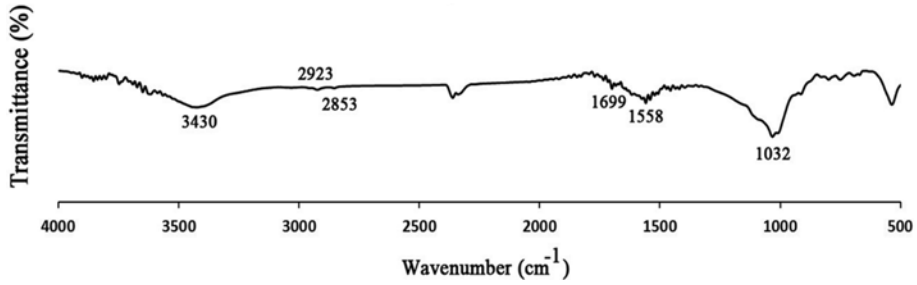


**Fig. 5. FTIR spectra of the AC sample.**

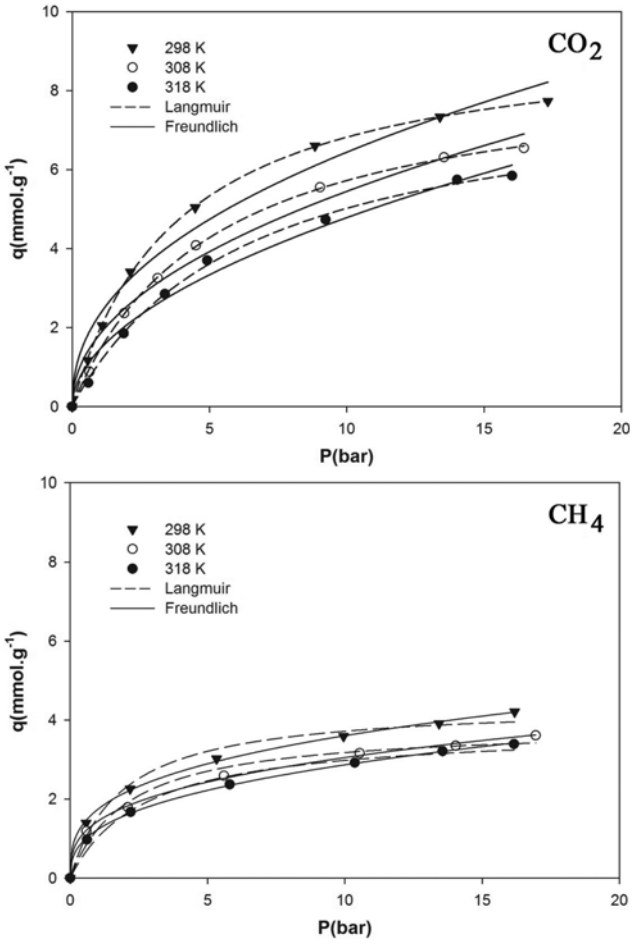


**Fig. 6. Nonlinear fit of experimental data with Langmuir and Freundlich models.**

molecular sieve the diffusion of smaller molecules occurs, while retaining the larger molecules.

The values of certain physicochemical properties of the adsorbate gases are listed in Table 3. The highest $CO_2$ adsorption can be attributed to its large quadrupole moment of $CO_2$ than $CH_4$ (non-polar), which strengthens the adsorbate-adsorbent interactions and, consequently, the adsorption in the structure increases. A similar behavior can be therefore expected during the adsorption of $CO_2/CH_4$ mixtures [38]. For molecules that are essentially spherical, such as $CH_4$, $d_k$ is very similar to the gas phase collision. Whereas, for linear and non-spherical molecules of $CO_2$ the kinetic diameter is closer to the minimum diameter of the molecule.

In transport phenomena, the molecule with the smallest kinetic diameter (dk) diffuses faster and behaves as the smallest one. Actually, the kinetic diameter of a gas molecule is close to the molecular sieving dimension and is considered as a sensitive measure of ability for moving in highly restrictive environments. According to Table 3, $CO_2$ has a smaller kinetic diameter than methane. Regarding separation by molecular sieving and considering the kinetic diameter of the $CO_2$ and $CH_4$ molecules, this activated carbon has more pore diameters smaller than 3.80 Å. Therefore, $CO_2$ can diffuse through the ultramicropores in activated carbon while remaining inaccessible to methane.

The $CO_2$ and $CH_4$ adsorption data were fitted to classical isotherm models, Langmuir and Freundlich. The comparison of experimental adsorption data of $CO_2$ and $CH_4$ in three temperatures with predicted values by Langmuir and Freundlich models is depicted in Fig. 6. The calculated adsorption parameters and the correlation coefficient ($R^2$) of all isotherms at 298, 308 and 318 K for the adsorption of $CO_2$ and $CH_4$ onto AC are summarized in Table 4.

The $R^2$ values from Table 4 show that Langmuir isotherm model yields a better fit to the experimental data ($R^2$>0.99) for $CO_2$ gas. In fact, $CO_2$ adsorption at monolayer coverage occurred on the AC surface with no important intermolecular interaction with neighboring adsorbed molecules. Whereas, the regression coefficients of the Freundlich model for $CH_4$ were more close to unity as compared to that of Langmuir isotherm, confirming better fitting of this isotherm model and multilayer adsorption of $CH_4$ on this

**Table 3. Physical properties of the $CO_2$ and $CH_4$ [23,24]**

| | Molecular weight, M (g·mol$^{-1}$) | Critical temperature, $T_c$ (K) | Permanent electric dipolar moment, $\mu_e$ (Debye) | Polarizability | Quadrupole moment, $q_m$ (esu·cm$^{-2}$) | Kinetic diameter, $d_k$ (nm) | Collision diameter, $d_c$ (nm) |
|---|---|---|---|---|---|---|---|
| $CO_2$ | 44.01 | 304.1 | 0 | $29.11*10^{-25}$ | $4.3*10^{-26}$ | 0.33 | 0.400 |
| $CH_4$ | 16.043 | 190.6 | 0 | $25.93*10^{-25}$ | 0 | 0.38 | 0.382 |

**Table 4. Equilibrium model constants for $CO_2$ and $CH_4$ adsorption by prepared activated carbon sample**

| | Temperature (K) | Langmuir | | | Freundlich | | |
|---|---|---|---|---|---|---|---|
| | | $q_m$ (mmol·g$^{-1}$) | b | $R^2$ | K | n | $R^2$ |
| $CO_2$ | 298 | 9.464 | 0.258 | 0.999 | 2.325 | 2.260 | 0.978 |
| | 308 | 8.641 | 0.196 | 0.999 | 1.826 | 2.106 | 0.982 |
| | 318 | 8.218 | 0.157 | 0.998 | 1.444 | 1.922 | 0.984 |
| $CH_4$ | 298 | 4.414 | 0.533 | 0.980 | 1.7371 | 3.153 | 0.999 |
| | 308 | 3.846 | 0.474 | 0.979 | 1.4366 | 3.059 | 0.999 |
| | 318 | 3.778 | 0.373 | 0.984 | 1.2291 | 2.719 | 0.999 |

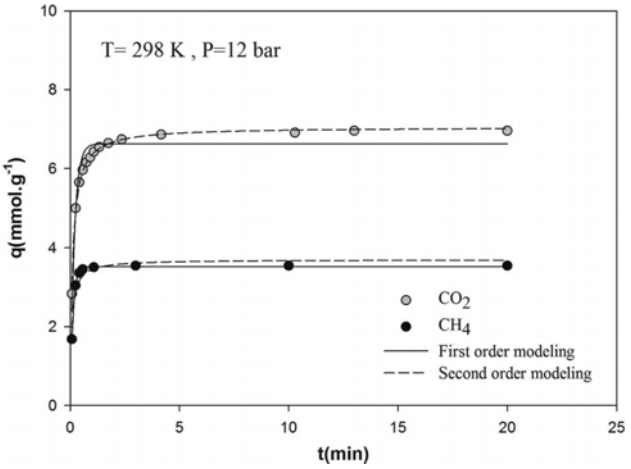


**Fig. 7. Kinetics of $CO_2$ and $CH_4$ adsorption by pine cone-based AC at 298 K.**

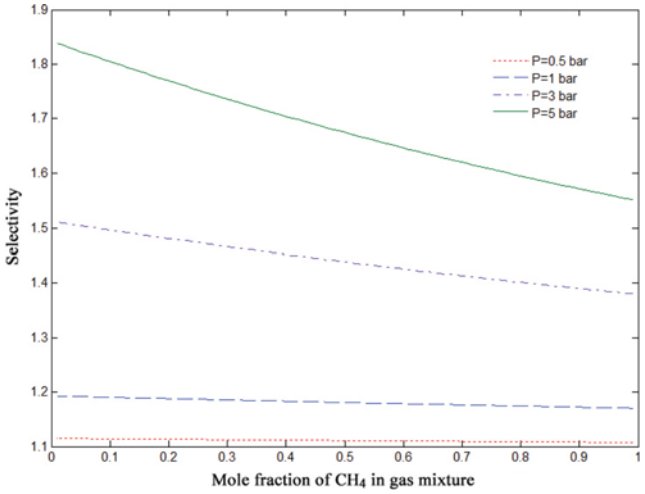


**Fig. 8. Ideal selectivity of $CO_2$ to $CH_4$ adsorbed on AC at 298 K and different pressures.**

adsorbent. For both gases, the Langmuir constant (b) values decrease with increasing in temperature from 298 to 318 K, indicating that there is lower affinity of $CO_2$ and $CH_4$ for AC at higher temperature. The maximum adsorption capacities estimated from the Langmuir equation ($q_m$) for $CO_2$ and $CH_4$ decreased with temperature, which indicated exothermic adsorption of these gases on to the AC. Also, the amount of this parameter for $CO_2$ was more than twice, indicating good affinity between $CO_2$ molecules and adsorbent rather than $CH_4$. The values of K decreased slightly from 298 to 318 K, indicating the reduction in the adsorption capacity at higher temperature. This is in agreement with Langmuir isotherm model observations. The values of constant n were higher than unity (Table 4), suggesting the feasibility of $CO_2$ and $CH_4$ adsorption onto the surface of AC.

**3. Kinetic Study**

A kinetic study of $CO_2$ and $CH_4$ adsorption by the AC prepared from pine cone at 298 K and 12 bar is depicted in Fig. 7. The plots of $q_t$ versus t showed that the adsorption capacity of $CO_2$ and $CH_4$ increased with time and attained a maximum value and, thereafter, it reached a constant value, indicating that no more gas molecules were further adsorbed on the adsorbent. The adsorption kinetics of both gases on prepared activated carbon consisted of two steps, a rapid step where gas adsorption was fast, and a slow step where the adsorbent was saturated by the adsorbate. The fast gas uptake at the initial stage may be due to the availability of the uncovered surface area and the vacant active sites on the adsorbent. In addition, with increasing the number of gas adsorbed molecules, the number of available adsorption sites was reduced. Consequently, the gas adsorption becomes almost constant after a short time for both gases, especially for $CH_4$.

The recorded data revealed that the adsorption time scale for carbon dioxide is longer than that for methane. This is because the equilibrium adsorption capacity of $CO_2$ by prepared adsorbent is higher than that of $CH_4$; therefore, it takes longer time to equilibrate the surface with $CO_2$. Another reason is attributed to the higher molecular weight of carbon dioxide rather than methane; hence the mobility of carbon dioxide in the gas space is slower than methane. In addition, due to the higher affinity of carbon dioxide towards the activated carbon, surface diffusivity of $CO_2$ is smaller than $CH_4$. Therefore, the mobility of the adsorbed carbon dioxide molecules is slower [39].

Adsorption kinetics data were investigated by using pseudo-first-order and pseudo-second-order kinetic models. The obtained parameters for theses two kinetic models are shown in Table 5. For carbon dioxide, the $q_e$ (exp) and the $q_e$ (cal) values from the pseudo-second-order kinetic model are very close to each other. In addition, the calculated correlation coefficients, ($R^2$) are also closer to unity for this kinetic model than that for the pseudo first-order kinetics. Therefore, the $CO_2$ adsorption by prepared AC can be approximated more appropriately by the pseudo-second-order kinetic model than the first-order kinetic model. Whereas, the values obtained with kinetic model of pseudo-first order are in agreement with experimental data for methane. The values of adsorption rate constants ($K_1$ and $K_2$) for gas adsorption on AC indicate that the rate of methane adsorption is fastest on AC than carbon dioxide due to the reasons that were mentioned above.

**4. Selectivity**

The ideal adsorbed solution theory (IAST) was applied to predict the $CO_2/CH_4$ selectivity from the experimental pure gas iso-

**Table 5. Constants of pseudo-first and second-order kinetics for the adsorption of $CO_2$ and $CH_4$ on AC**

| | $q_e$ (exp) | First order | | | Second order | | |
|---|---|---|---|---|---|---|---|
| | | $K_1$ | $q_e$ (cal) | $R^2$ | $K_2$ | $q_e$ (cal) | $R^2$ |
| $CO_2$ | 6.95 | 5.374 | 6.63 | 0.935 | 1.276 | 7.05 | 0.996 |
| $CH_4$ | 3.54 | 7.791 | 3.52 | 0.999 | 3.705 | 3.70 | 0.919 |

therms under mixture conditions by using Langmuir isotherm parameters. The predicted selectivity of $CO_2$ to $CH_4$ from IAST as a function of compositions and at different pressures for prepared AC is shown in Fig. 8. At constant temperature, selectivity increased with increasing the pressure because of behavior of the system that arises from the appropriate pore size toward the carbon dioxide molecule size. Actually, based on the two main mechanisms for adsorption selectivity which are kinetic separation and thermodynamic separation, $CO_2$ has smaller kinetic diameter, higher quadrupole moment and higher polarizability compared to $CH_4$ which in many cases results in stronger interaction with pore surface of the adsorbent. The adsorption selectivity of $CO_2$ over $CH_4$ on AC ($CO_2$ : $CH_4$=50 : 50, 298 K, 5 bar) was achieved at 1.68.

**5. Thermodynamics of Adsorption**

The amount of heat of adsorption determines the type of physical and chemical adsorption. In physical adsorption, the gas molecule is adsorbed to the solid surface by weak van der Waals and electrostatic interactions. Whereas, a strong chemical bond is formed between the adsorbent and adsorbate in chemical adsorption. For heat of adsorption of 80 kJ·mol$^{-1}$ or more, the adsorption process indicates chemisorption, while lower values represent a physical adsorption phenomenon [40,41].

The isosteric heat of $CO_2$ and $CH_4$ adsorption onto AC was determined from the slope of the lines of lnP versus 1/T plot at a constant adsorbed amount (Fig. 9). The negative slopes shown in Fig. 9 confirmed the exothermic of the adsorption process of both gases by AC. In Fig. 10, the heat of adsorption for $CO_2$ and $CH_4$ by prepared AC is depicted as a function of surface loading. For $CO_2$, the isosteric heat of adsorption demonstrates almost constant at lower surface coverage, suggesting a homogeneous adsorption system, and there is molecular interaction between the adsorbed $CO_2$ molecules. With increasing $CO_2$ loading, the isosteric heat increases slightly due to the adsorbate-adsorbate interactions at higher pressure.

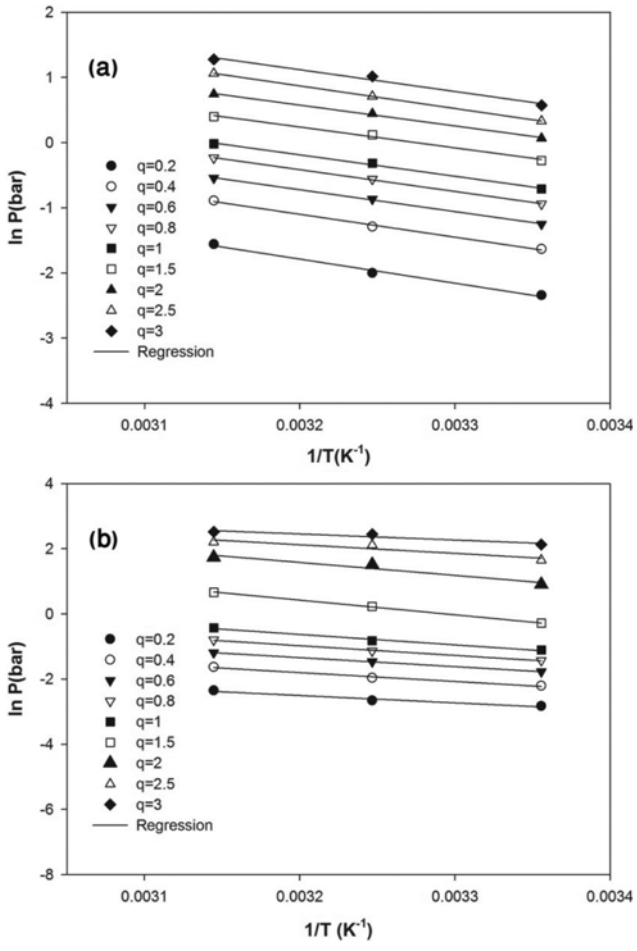


**Fig. 9. Isosteric heat of adsorption of $CO_2$ (a) and $CH_4$ (b) on the AC (q in mmol g$^{-1}$).**

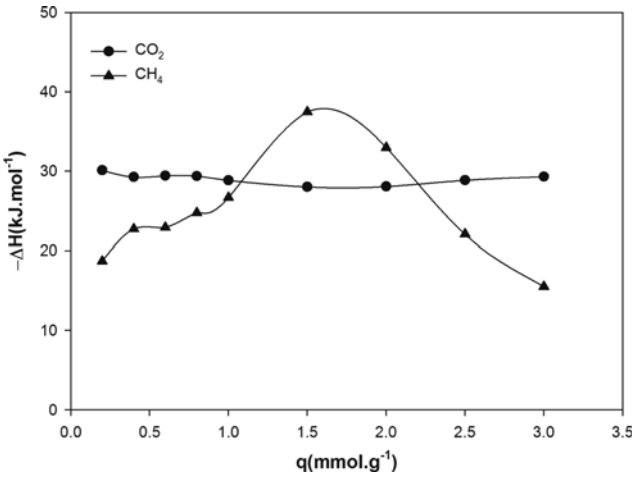


**Fig. 10. Isosteric heat of adsorption against surface loading for adsorption of $CO_2$ and $CH_4$ onto AC.**

From Fig. 10, at lower surface loading the variation of the isosteric heat of adsorption with the amount of adsorbed $CH_4$ was increased. This can be explained by knowing that at lower pressure, $CH_4$ molecules can come into direct contact with the adsorbent due to low surface coverage. Also, adsorbate-adsorbate interaction occurs between $CH_4$ molecules with increase in the surface loading. However, at high surface coverage (from 1.5 mmol·g$^{-1}$ up to 3 mmol·g$^{-1}$), a weak interaction between $CH_4$ and adsorbent occurs. Since, the strong adsorption sites are occupied first and upon increased loading, the weaker adsorption sites will be occupied. Hence, the heat of adsorption decreases. These results are compatible with the results obtained from the Freundlich isotherm, which was consistent for $CH_4$ adsorption. The isosteric heat values, obtained for both gases, were lower than 80 kJ·mol$^{-1}$ confirming the physical interactions between gases and the prepared sorbent. In lower surface coverage, the $\Delta H_{st}$ value for carbon dioxide was higher than that for methane, which indicates that carbon dioxide is significantly strongly adsorbed on the AC than the methane and the availability of adsorption sites for $CO_2$ on AC is more than $CH_4$.

The values of $\Delta H^0$ and $\Delta S^0$ were measured from the slope and the intercept of the linear plot of $\Delta G^0$ versus T and presented in Table 6. The negative $\Delta G^0$ values for both gases at various temperatures verified the feasibility of the process and the spontaneous nature of these gases onto prepared AC. With increasing the temperature, $\Delta G^0$ was increased, indicating that $CO_2$ and $CH_4$ adsorption are exothermic and more favorable at lower temperature. The

**Table 6. Thermodynamic parameters for $CO_2$ adsorption onto prepared AC**

| Gas | $q_e$ (mmol·g$^{-1}$) | ΔS (J·mol$^{-1}$ K$^{-1}$) | ΔG (kJ·mol$^{-1}$) | | | ΔH (kJ·mol$^{-1}$) |
|---|---|---|---|---|---|---|
| | | | 298 | 308 | 318 | |
| $CO_2$ | 0.2 | −76.2 | −5.780 | −5.109 | −4.255 | −28.533 |
| | 0.4 | −79.4 | −4.012 | −3.278 | −2.423 | −27.708 |
| | 0.6 | −83.0 | −3.101 | −2.221 | −1.440 | −27.833 |
| | 0.8 | −85.5 | −2.333 | −1.439 | −0.623 | −27.799 |
| | 1 | −85.7 | −1.767 | −0.806 | −0.053 | −27.271 |
| $CH_4$ | 0.2 | −39.4 | −7.012 | −6.810 | −6.223 | −18.832 |
| | 0.4 | −58.0 | −5.469 | −5.035 | −4.309 | −22.802 |
| | 0.6 | −62.1 | −4.390 | −3.763 | −3.148 | −22.894 |
| | 0.8 | −71.3 | −3.536 | −2.918 | −2.111 | −24.800 |
| | 1 | −80.4 | −2.747 | −2.102 | −1.139 | −26.759 |

more negative values of Gibbs free energy indicates a greater driving force to the adsorption process. When the temperature increases, the $\Delta G^0$ values decrease, representing less driving force and hence adsorption capacity at higher temperatures decreases [42].

As a rule of thumb, a process with $\Delta G^0$ change ranges up to –40 kJ·mol$^{-1}$ are taken into account to be controlled by chemisorption, while $\Delta G^0$ change ranges up to −20 kJ·mol$^{-1}$ indicate physisorption [43]. The amounts of $\Delta G^0$ values obtained for $CO_2$ and $CH_4$ were lower than −20 kJ·mol$^{-1}$. This indicates that the process of $CO_2$ and $CH_4$ adsorption on the prepared AC used in this study was dominated by physisorption. The negative value of $\Delta H^0$ for both gases suggest that the gas-AC interaction is exothermic, which was the reason for the increase in adsorption at lower temperature. The values of enthalpy for both gases were lower than 40 kJ·mol$^{-1}$, confirming the physisorption of the adsorption process. At surface loading of 0.2 to 1, the enthalpy of $CO_2$ was almost constant, indicating the homogeneous adsorption surfaces. These results were also in good agreement with the isosteric heat obtained for $CO_2$ at a constant adsorbate loading. Unlike $CO_2$, for $CH_4$ the obtained values of enthalpy are very close to the values obtained from isosteric heat of absorption at a constant adsorbate loading. Also, the enthalpy value for $CH_4$ increases slightly with increasing surface coverage, attributed to adsorbate-adsorbate interaction followed by adsorbate-adsorbent interaction.

Negative entropy change corresponds to a reduction in degree of freedom of the adsorbed gas. Therefore, when the concentration of adsorbate in solid-gas interface decreases, the adsorbate amount onto the solid phase increases. As shown in Table 6, with increasing the surface coverage, −ΔS had enhancement because of the increasing in the adsorbate concentration onto the solid phase. It is also evident that the higher values of entropy for the $CO_2$ in comparison with $CH_4$ at the same surface loading are due to the stronger adsorption of $CO_2$ molecules with AC (adsorbate-adsorbent interactions) in lower surface coverage. This stronger adsorption causes a higher loss of mobility of the $CO_2$ molecules (it means higher interaction between the molecule and the surface).

## CONCLUSION

Activated carbon was prepared from chemical activation of pine cone by $H_3PO_4$ and used for $CO_2$ and $CH_4$ adsorption equilibrium in the temperature range of 298-318 K and pressure range of 1-16 bar. The synthesized activated carbon showed well-developed porosity and high surface area. The BET surface area and total pore volume of pine cone-based AC were 1,470 m$^2$/g and 0.6415 cm$^3$/g, respectively. Experimental results were analyzed through Langmuir and Freundlich models, which led to estimating the relative performance of these two isotherm models, describing the experimental results, quantifying the gas adsorption on prepared AC and classifying them. The kinetic results show that adsorption time for carbon dioxide is longer than that for methane. The adsorption selectivity of $CO_2$ over $CH_4$ on AC ($CO_2$ : $CH_4$=50 : 50, 298 K, 5 bar) based on the IAST was achieved at 1.68. The results revealed that pine cone activated carbon prepared using phosphoric acid is selective to carbon dioxide, which makes it a very good candidate for capture of $CO_2$ from natural gas.

## REFERENCES


1. Z. H. Rada, H. R. Abid, J. Shang, Y. He, P. Webley, S. Liu, H. Sun and S. Wang, *Fuel*, **160**, 318 (2015).
2. S. Gilassi and N. Rahmanian, *Appl. Math. Model.*, **39**, 6599 (2015).
3. H. Halim, A. Shariff and M. Bustam, *Sep. Purif. Technol.*, **152**, 87 (2015).
4. S. S. A. Talesh, S. Fatemi, S. Hashemi and M. Ghasemi, *Sep. Sci. Technol.*, **45**, 1295 (2010).
5. G. K. Parshetti, S. Chowdhury and R. Balasubramanian, *Fuel*, **148**, 246 (2015).
6. L. Guo, X. Hu, G. Hu, J. Chen, Z. Li, W. Dai, H. F. Dacosta and M. Fan, *Fuel Process. Technol.*, **138**, 663 (2015).
7. J. L. Spenik, L. J. Shadle, R. W. Breault, J. S. Hoffman and M. L. Gray, *Ind. Eng. Chem. Res.*, **54**, 5388 (2015).
8. B. S. Caglayan and A. E. Aksoylu, *J. Hazard. Mater.*, **252-253**, 19 (2013).
9. Q. Zhou, Y.-F. Duan, Y.-G. Hong, C. Zhu, M. She, J. Zhang and H.-Q. Wei, *Fuel Process. Technol.*, **134**, 325 (2015).
10. V. K. Gupta, D. Pathania, S. Sharma and P. Singh, *J. Colloid Interface Sci.*, **401**, 125 (2013).
11. M. Momčilović, M. Purenović, A. Bojić, A. Zarubica and M. Ranđelović, *Desalination*, **276**, 53 (2011).

12. D. J. Malik, V. Strelko Jr., M. Streat and A. M. Puziy, *Water Res*., **36**, 1527 (2002).
13. V. Boonamnuayvitaya, C. Chaiya, W. Tanthapanichakoon and S. Jarudilokkul, *Sep. Purif. Technol*., **35**, 11 (2004).
14. A. C. Martins, O. Pezoti, A. L. Cazetta, K. C. Bedin, D. A. Yamazaki, G. F. Bandoch, T. Asefa, J. V. Visentainer and V. C. Almeida, *Chem. Eng. J*., **260**, 291 (2015).
15. W. C. Lim, C. Srinivasakannan and A. Al Shoaibi, *J. Clean. Prod*., **102**, 501 (2015).
16. T. Bohli, A. Ouederni, N. Fiol and I. Villaescusa, *Comptes. Rendus. Chimie*., **18**, 88 (2015).
17. S. Dawood, T. K. Sen and C. Phan, *Water Air Soil Pollut*., **225**, 1 (2014).
18. M. Brebu, S. Ucar, C. Vasile and J. Yanik, *Fuel*, **89**, 1911 (2010).
19. C. Saucier, M. A. Adebayo, E. C. Lima, R. Cataluña, P. S. Thue, L. D. Prola, M. Puchana-Rosero, F. M. Machado, F. A. Pavan and G. Dotto, *J. Hazard. Mater*., **289**, 18 (2015).
20. O. Pezoti, A. L. Cazetta, I. P. Souza, K. C. Bedin, A. C. Martins, T. L. Silva and V. C. Almeida, *J. Ind. Eng. Chem*., **20**, 4401 (2014).
21. W. C. Lim, C. Srinivasakannan and N. Balasubramanian, *J. Anal. Appl. Pyrol*., **88**, 181 (2010).
22. M. Açıkyıldız, A. Gürses, K. Güneş and D. Yalvaç, *Appl. Surf. Sci*., **354**, 279 (2015).
23. M. Kilic, E. Apaydin-Varol and A. E. Pütün, *J. Hazard. Mater*., **189**, 397 (2011).
24. S. Wang, T. Terdkiatburana and M. Tadé, *Sep. Purif. Technol*., **62**, 64 (2008).
25. S. Kaur, S. Rani, R. Mahajan, M. Asif and V. K. Gupta, *J. Ind. Eng. Chem*., **22**, 19 (2015).
26. Y. Keren, M. Borisover and N. Bukhanovsky, *Chemosphere*, **138**, 462 (2015).
27. M. A. Sheikh, M. M. Hassan and K. F. Loughlin, *Gas Sep. Purif*., **10**, 161 (1996).
28. R.-L. Tseng, P.-H. Wu, F.-C. Wu and R.-S. Juang, *Chem. Eng. J*., **237**, 153 (2014).
29. L. Kong, R. Zou, W. Bi, R. Zhong, W. Mu, J. Liu, R. P. Han and R. Zou, *J. Mater. Chem. A*, **2**, 17771 (2014).
30. J.-R. Li, J. Sculley and H.-C. Zhou, *Chem. Rev*., **112**, 869 (2011).
31. A. Myers and J. M. Prausnitz, *AIChE J*., **11**, 121 (1965).
32. C. Yu, M. G. Cowan, R. D. Noble and W. Zhang, *Chem. Commun*., **50**, 5745 (2014).
33. W. Luerruk, A. Shotipruk, V. Tantayakom, P. Prasitchoke and C. Muangnapoh, *Front. Chem. Eng. China*, **3**, 52 (2009).
34. S. Khalili, A. A. Ghoreyshi, M. Jahanshahi and K. Pirzadeh, *CLEAN-Soil, Air, Water*, **41**, 939 (2013).
35. P. Justin, *Hydrogen adsorption by alkali metal graphite intercalation compounds*, Diss. California Institute of Technology (2010).
36. M. Loredo-Cancino, E. Soto-Regalado, F. Cerino-Córdova, R. García-Reyes, A. García-León and M. Garza-González, *J. Environ. Manag*., **125**, 117 (2013).
37. Z.-Y. Zhong, Q. Yang, X.-M. Li, K. Luo, Y. Liu and G.-M. Zeng, *Ind. Crop. Prod*., **37**, 178 (2012).
38. Y.-S. Bae, O. K. Farha, J. T. Hupp and R. Q. Snurr, *J. Mater. Chem*., **19**, 2131 (2009).
39. I. Prasetyo and D. Do, *Chem. Eng. Sci*., **53**, 3459 (1998).
40. S. Khalili, A. A. Ghoreyshi and M. Jahanshahi, *Chem. Ind. Chem. Eng. Quart*., **19**, 153 (2013).
41. M. Cinke, J. Li, C. W. Bauschlicher, A. Ricca and M. Meyyappan, *Chem. Phys. Lett*., **376**, 761 (2003).
42. M. H. Kalavathy, T. Karthikeyan, S. Rajgopal and L. R. Miranda, *J. Colloid Interface Sci*., **292**, 354 (2005).
43. T. Anirudhan and P. Radhakrishnan, *Chem. Eng. J*., **165**, 142 (2010).